PARTICLE INFLUX MEASUREMENTS WITH THE ASDEX-UPGRADE MULTICHORD VISIBLE SPECTROSCOPY SYSTEM

A. Kallenbach, H.-M. Mayer, W. Schneider

IPP 1/265 Januar 1992

MAX-PLANCK-INSTITUT FÜR PLASMAPHYSIK

8046 GARCHING BEI MÜNCHEN

MAX-PLANCK-INSTITUT FÜR PLASMAPHYSIK

GARCHING BEI MÜNCHEN

PARTICLE INFLUX MEASUREMENTS WITH THE ASDEX-UPGRADE MULTICHORD VISIBLE SPECTROSCOPY SYSTEM

A. Kallenbach, H.-M. Mayer, W. Schneider

IPP 1/265 Januar 1992

Die nachstehende Arbeit wurde im Rahmen des Vertrages zwischen dem Max-Planck-Institut für Plasmaphysik und der Europäischen Atomgemeinschaft über die Zusammenarbeit auf dem Gebiete der Plasmaphysik durchgeführt.

January 29, 1992

Particle influx measurements with the ASDEX-Upgrade multichord visible spectroscopy system

A. Kallenbach, H.-M. Mayer, W. Schneider

Max-Planck-Institut für Plasmaphysik

D–8046 Garching, Federal Republic of Germany

EURATOM–IPP Association

Abstract

This report describes the hardware and software components of the ASDEX-Upgrade multichord visible spectroscopy system. Main emphasis is laid on a detailed description of the detector, a free programmable charge-coupled device intensified by a microchannel plate. As an experimental application, flux measurements of different impurity species from the inner heat shield are presented. Poloidal profiles of the released impurity amount obtained for various experimental situations are used to check the plasma position which is derived by the function parametrization analysis.

I. Introduction

Although thermal photon emission from the bulk of today's tokamak plasmas occurs predominantly in the soft-X range, visible spectroscopy remains an important diagnostic tool. The two main applications are

i determination of particle fluxes into the plasma from the emission of low ionized species

ii measurement of bulk temperatures, ion densities and rotation velocities by means of charge exchange recombination spectroscopy (CXRS) during neutral beam injection.

Both applications naturally demand a multichordal detection system, either to measure at different positions on the limiting wall or to obtain profiles as a function of the flux coordinate. This report describes a new diagnostic system, which is able to record highly resolved spectra in the visible and near-UV range with an appropriate sensitivity, speed and channel number. As an experimental application, the influx of different atomic species under various experimental conditions in the ASDEX-Upgrade tokamak[1] is presented.

II. Experimental setup

The principal setup of the diagnostic system is shown in Fig. 1. Light emitted along 12 viewing lines in a poloidal plane of the plasma is collected by a quartz lens (f=0.3 m) and imaged onto 12 fiber guides. Each fiber guide (referred to as 'channel' in the following) consists of 2 quartz fibers (Fiberguide Industries, Superguide B PCS) transmitting the light to the spectrograph over a distance of 23 m and through the radiation shield wall. The core/clad/jacket diameters of an individual fiber are 400/420/470 μm, respectively. The configuration of the fibers in front of the entrance slit of the spectrograph is shown in Fig. 2. The mean diameter of the elliptical viewing cones on the limiter is about 1 cm. During the 1991 experimental period, only channel number 2-11 had optical access to the heat shield at torus port 11. The arrangement of the lines with respect to the plasma boundary is shown in Fig. 3. Full optical access to the whole height

of the heat shield will be available in torus port 13 at the beginning of the 1992 experimental period.

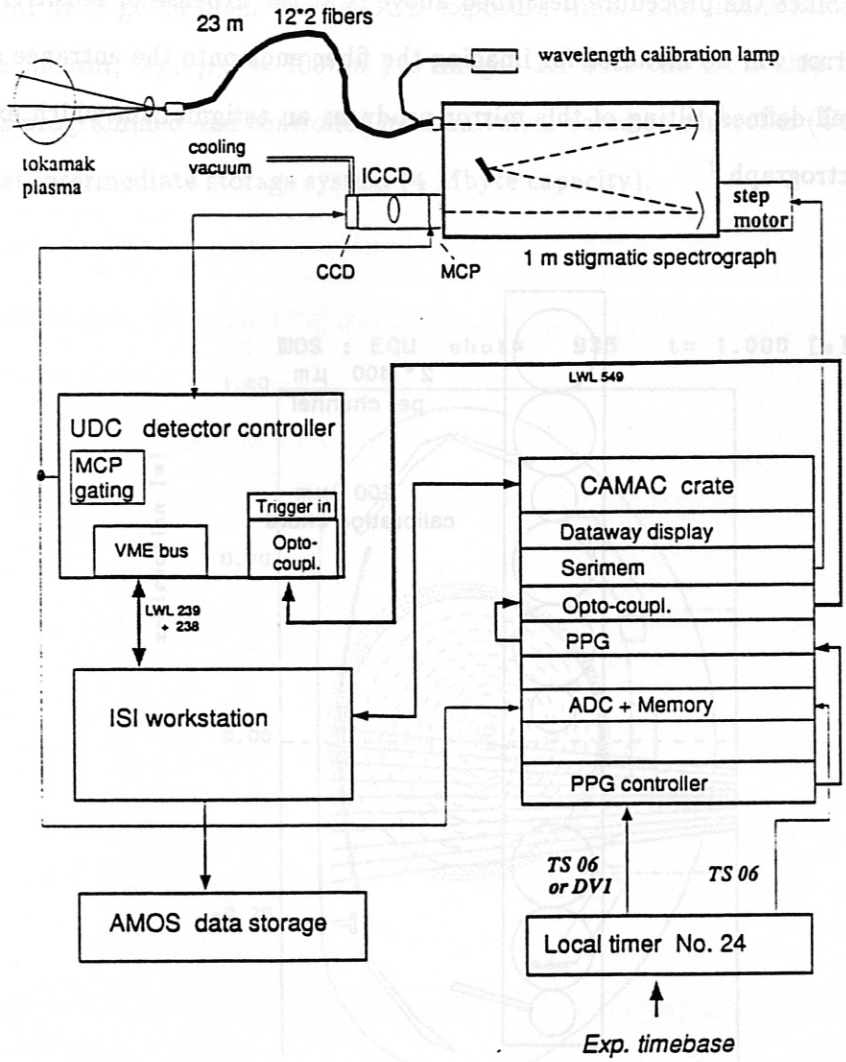

Figure 1: *Principal setup of the visible multichord diagnostic system.*

When imaging the fiber output onto the spectrograph entrance slit, the astigmatism of the spectrograph resulting from the different reflection angles of the spherical mirrors in horizontal and vertical direction has to be taken into account: in contrast to typical photomultiplier- or linear array configurations, a high spatial resolution along the direction of the entrance slit is

desired in the output plane of the spectrograph. To compensate for the astigmatism, the fibers were simply placed 7 mm in front of the entrance slit in the vertical focal plane. As usual, the spectrograph is adjusted to produce a sharp image of the entrance slit in the horizontal (i.e. wavelength) direction. Since the procedure described above is at the expense of sensitivity, an additional spherical mirror will be installed for imaging the fiber ends onto the entrance slit of the spectrograph. A well-defined tilting of this mirror produces an astigmatism which exactly cancels that of the spectrograph.[2]

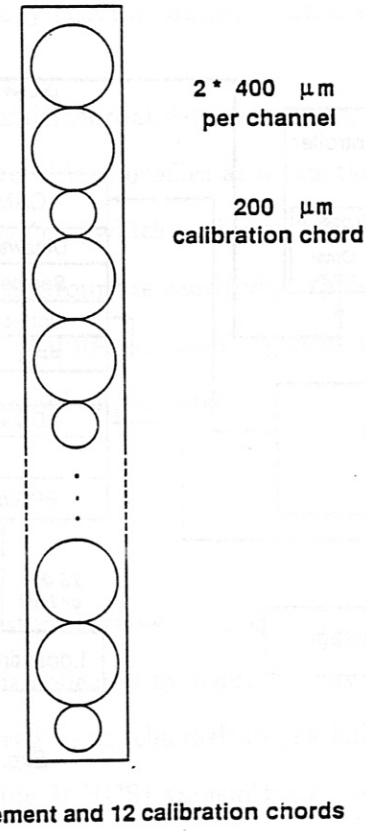

Figure 2: *Fiber configuration in front of the entrance slit of the spectrograph. Each couple of 2 thick fibers 400 µm in diameter forms one of the 12 channels. The 12 channels are separated by smaller fibers (d= 200µm), which are connected to a spectral lamp for wavelength calibration.*

The output plane of the spectrograph is equipped with a semi-commercial detection system

(B&M Spektronik) consisting of an image intensifier (Varo, Inc.), a lens system (Zeiss), a CCD-chip (Thomson CSF) and readout electronics. The image intensifier placed directly in the focal plane of the spectrograph is mainly used as a shutter for the CCD and operated with low gain. It is gated open during CCD exposure time. The intensifier screen (P20 phosphor, $\lambda_{max} \approx 550nm$, $\lambda_{FWHM} = 100nm$) is imaged 1:1 onto the CCD chip by a lens system. The CCD is programmed and controlled by a universal detector controller (UDC), which also serves as a fast intermediate storage system (4 Mbyte capacity).

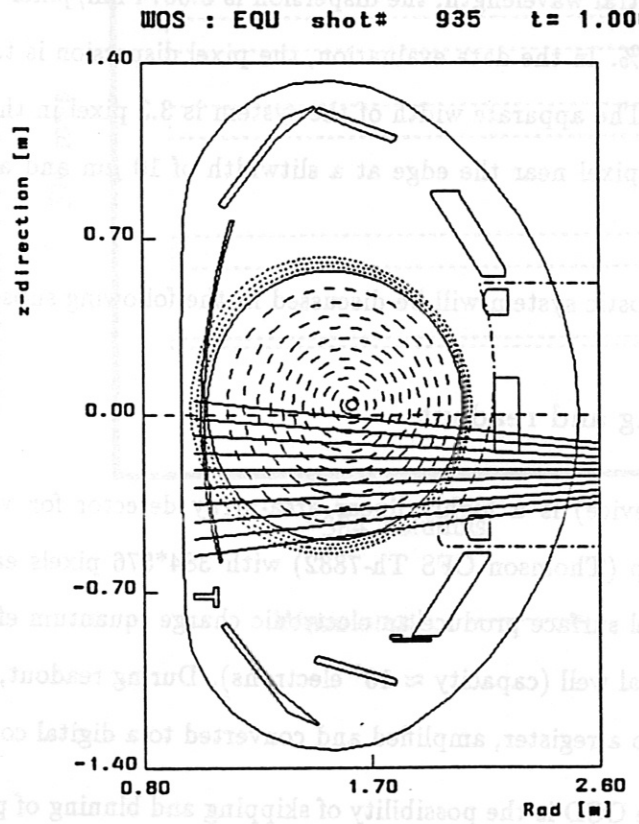

Figure 3: *Arrangement of the viewing lines with respect to the last closed flux surface of a circular limiter plasma. Channel numbers are 2 - 11 from top to bottom.*

To reduce the dark count rate, the CCD chip is cooled down to - 30° Celsius by means of a water

cooled multistage Peltier element. The camera is evacuated twice a month in order to maintain the thermal insulation of the CCD and to prevent the formation of clouding.

The detector controller is programmed and read out by a Unix workstation (Integrated Solutions) via a VME bus interface. Required trigger pulses (at least a single start trigger pulse) are generated by a programmable pulse generator (PPG) based in a CAMAC crate which is also connected to the host computer. The PPG is initialized by the ASDEX-Upgrade timer system to ensure a fixed coupling to the general experimental time base.

The full spectral width of the system, equipped with a 2400 grooves/mm grating, is 2.833 nm at λ=468.5 nm. For this central wavelength, the dispersion is 0.0074 nm/pixel with a measured variation of less than $\pm$ 0.5 %. In the data evaluation, the pixel dispersion is taken constant at a fixed central wavelength. The apparate width of the system is 3.3 pixel in the central part of the CCD chip and up to 4 pixel near the edge at a slitwidth of 10 μm and a groupsize of 20 pixel.

Further details of the diagnostic system will be discussed in the following subsections.

A. CCD programming and readout

A CCD (charge-coupled device) is a highly linear area-array detector for visible light. We use a front illuminated chip (Thomson CFS Th-7882) with 384*576 pixels each 23*23 μm in size. Photons hitting a pixel surface produce an electronic charge (quantum efficiency $\approx$ 30 %) which is stored in a potential well (capacity $\approx 10^6$ electrons). During readout, the charge of an individual pixel is shifted to a register, amplified and converted to a digital count number.

An important feature of the CCD is the possibility of skipping and binning of pixels during chip readout. When the CCD is used as a detector in the focal plane of a stigmatic spectrograph, skipping and binning allows to match the number of channels and the required spectral cut for a specific diagnostic application easily by software programming.

Fig. 4 illustrates a typical configuration of the chip. Each channel stripe corresponds to an optical fiber bundle with a certain viewing direction. The marked readout areas match the fiber

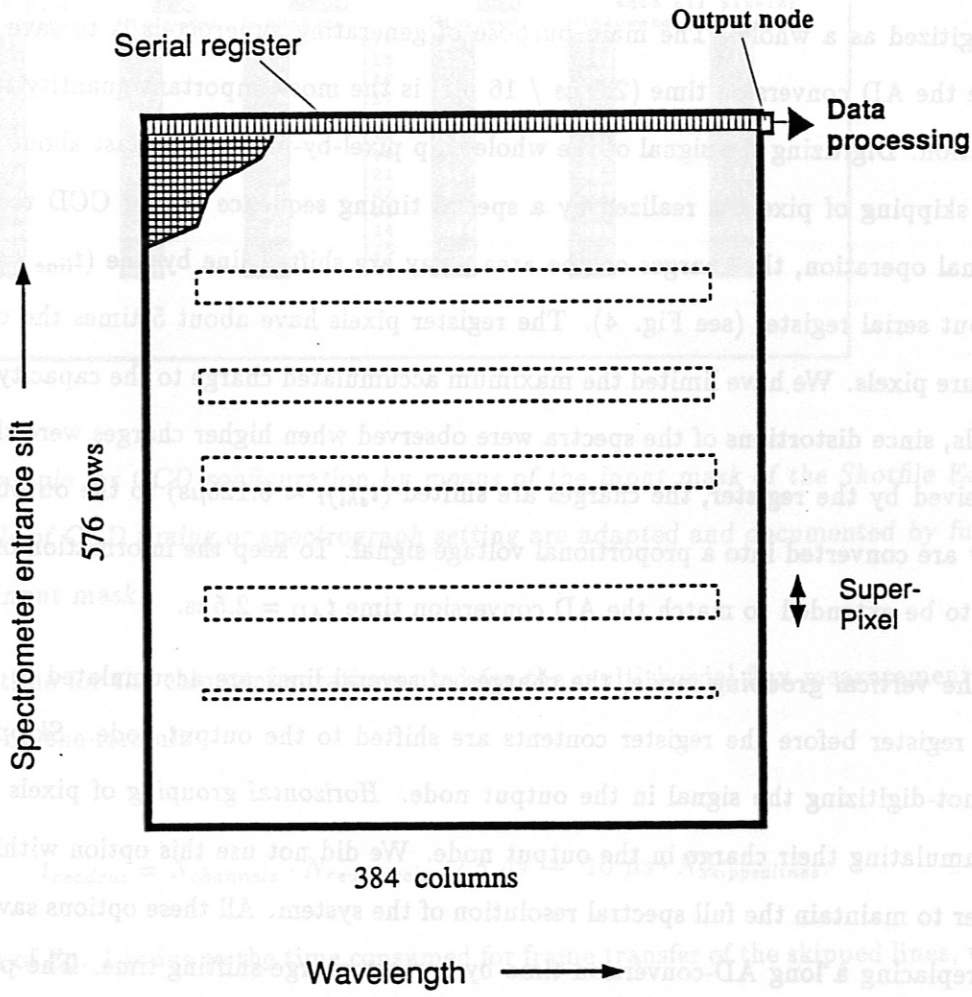

Figure 4: *Configuration of the CCD chip. The dashed rectangles represent superpixels obtained by vertical binning. Readout is done by frame transfer into the serial register, which is then shifted pixel by pixel into the output node*

guides at the entrance slit in their vertical positions. The definition of the pixels which are actually used is obtained by skipping and binning of pixels during CCD readout. Usually, 20-40 pixels of a channel stripe are binned together in vertical direction forming a superpixel which is digitized as a whole. The main purpose of generating superpixels is to save readout time, since the AD conversion time (2.5 μs / 16 bit) is the most important quantity for the readout duration. Digitizing the signal of the whole chip pixel-by-pixel would last about 0.6 s. Binning and skipping of pixels is realized by a special timing sequence during CCD readout. During normal operation, the charges on the area array are shifted line by line ($t_{line} \approx 1\mu s$) into the output serial register (see Fig. 4). The register pixels have about 5 times the capacity of the picture pixels. We have limited the maximum accumulated charge to the capacity of the picture pixels, since distortions of the spectra were observed when higher charges were shifted.
Received by the register, the charges are shifted ($t_{shift} \approx 0.125\mu s$) to the output node, where they are converted into a proportional voltage signal. To keep the information of a pixel, t_{shift} has to be extended to match the AD conversion time $t_{AD} = 2.5\mu s$.

In the *vertical grouping* mode, the charges of several lines are accumulated in the serial output register before the register contents are shifted to the output node. *Skipping* is realized by not-digitizing the signal in the output node. *Horizontal grouping* of pixels is achieved by accumulating their charge in the output node. We did not use this option within this work in order to maintain the full spectral resolution of the system. All these options save readout time by replacing a long AD-conversion time by a short charge-shifting time. The programming of chip array is easily done by using the mask input facility of the ASDEX-Upgrade Shotfile Editor (sfed). Fig. 5 shows a typical setup.

During each readout sequence, all pixel charges have to be transferred through the output node in order to erase the chip completely. The chip readout speed is increased considerably by accumulating succeeding lines which contain only skipping pixels in the serial register. However, this operational mode requires low illumination levels on the skipped areas of the chip to prevent a charge saturation of the serial register pixels. For the application presented in this paper, the required low illumination is assured by a proper fiber coupling.

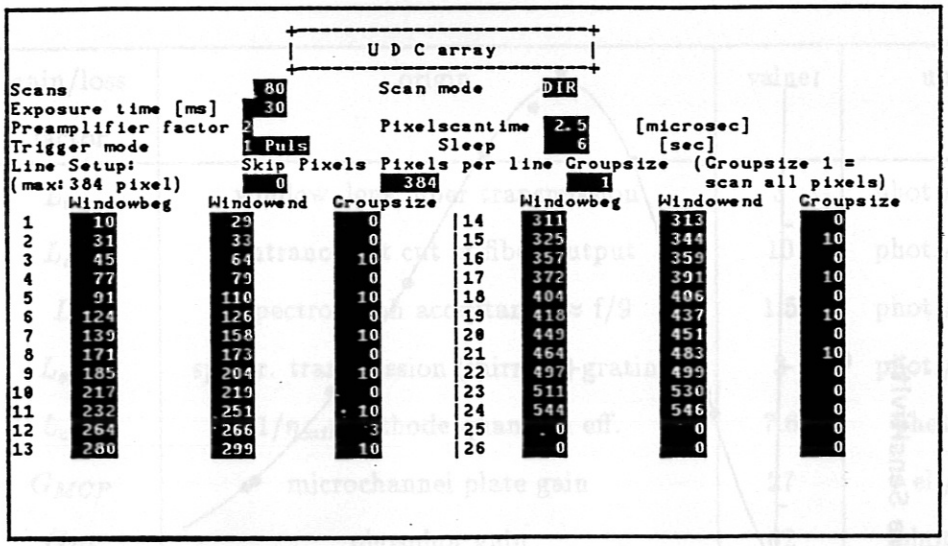

U D C array

Scans 80 Scan mode DIR
Exposure time [ms] 30
Preamplifier factor 2 Pixelscantime 2.5 [microsec]
Trigger mode 1 Puls Sleep 6 [sec]
Line Setup: Skip Pixels Pixels per line Groupsize (Groupsize 1 = scan all pixels)
(max: 384 pixel) 0 384 1

	Windowbeg	Windowend	Groupsize		Windowbeg	Windowend	Groupsize
1	10	29	0	14	311	313	0
2	31	33	0	15	325	344	10
3	45	64	10	16	357	359	0
4	77	79	0	17	372	391	10
5	91	110	10	18	404	406	0
6	124	126	0	19	418	437	10
7	139	158	10	20	449	451	0
8	171	173	0	21	464	483	10
9	185	204	10	22	497	499	0
10	217	219	0	23	511	530	0
11	232	251	10	24	544	546	0
12	264	266	3	25	0	0	0
13	280	299	10	26	0	0	0

Figure 5: *Example for CCD configuration by means of the input mask of the Shotfile Editor. Further details of CCD timing or spectrograph setting are adapted and documented by further pages of the input mask.*

The readout time for the chip configurations used for the multichordal flux measurements can be estimated by the formula

$$t_{readout} = N_{channels} \cdot N_{readpixels} \cdot 2.5\ \mu s\ +\ 10\ \mu s \cdot N_{skippedlines}. \quad (1)$$

The last term of Eq. 1 is due to the time consumed for frame transfer of the skipped lines, which is carried out in sections. For 11 channels with full (384 pixel) spectral coverage and groupsize gs= 20 pixels, we obtain $t_{readout}$ = 14.1 ms. The exposure time of the chip has to be added to the readout time to get the full cycle time for repetitive spectra recording.

B. Spectral response and signal-to-noise ratio

The complete detector system, including spectrograph, fiber coupling lens and quartz window has been calibrated by means of an optical diffuser (Oriel), illuminated by a continuous lamp (Osram Xenophot HLX, 100 W). The emissivity of the diffuser screen was measured at various

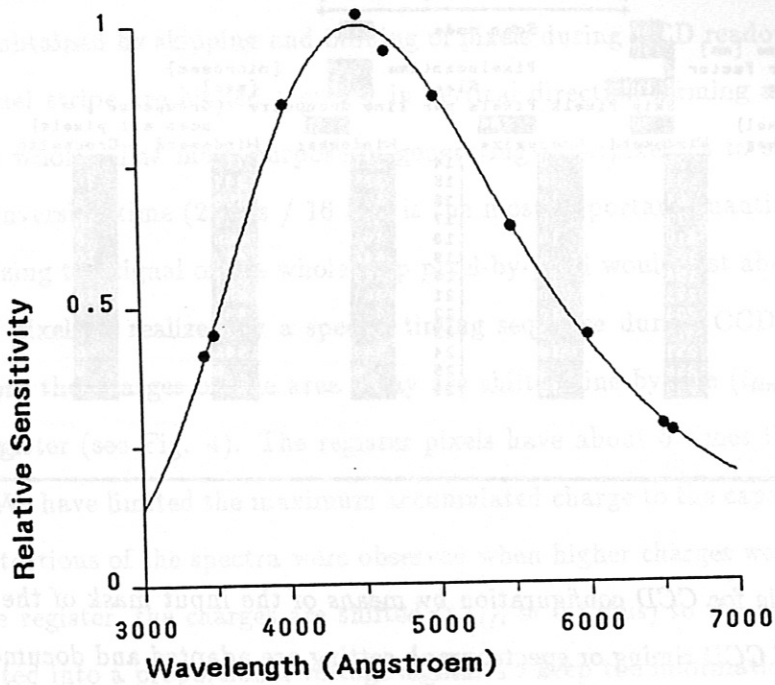

Figure 6: *Relative spectral sensitivity of the complete system. The peak value at λ=450 nm corresponds to the calibration factor of* $k = 8.3 \cdot 10^{12} \frac{Photons}{count \cdot m^2 \cdot sr \cdot nm \cdot s}$.

wavelengths over the spectral range of interest using a standard tungsten ribbon calibration lamp. The greater diameter of the screen in comparison to the calibrated area of the tungsten ribbon allows to calibrate in the original geometrical arrangement of the measurements.

The relative spectral response of the system for standard operational conditions (vertical groupsize gs=20, slitwidth sw=100 μm) is shown in Fig. 6. The groupsize gs=20 collects the light of one fiber, gs=40 is used for weak lines.

The peak sensitivity at λ=450 nm corresponds to the calibration factor $k = 8.3 \pm 1.5 \cdot 10^{12} \frac{Photons}{count \cdot m^2 \cdot sr \cdot nm \cdot s}$.

In the following, we estimate the performance of the system for $\lambda = 450nm$ and standard conditions part by part in order to highlight the features which limit the sensitivity and the signal-to-noise ratio.

gain/loss factor	origin	value	unit
L_{inp}	window, lens, fiber transmission	3	phot./phot.
L_{slit}	entrance slit cut of fiber output	10	phot./phot.
L_{Ω}	spectrograph acceptance $\approx$ f/9	1.5	phot./phot.
L_{spek}	spectr. transmission (mirrors+grating)	3	phot./phot.
L_{cath}	$1/\eta_{cath}$ cathode quantum eff.	7.6	phot./el.
G_{MCP}	microchannel plate gain	27	el./el.
G_{Ph}	phosphor gain	62	phot./el.
L_{coup}	phosphor-to-CCD coupling	7	phot./phot.

Table 1: Gain and loss factors from optical fiber input to CCD array for standard conditions.

The plasma volume of interest is imaged onto the fiber by a quartz lens (focal length f=0.3 m, effective diameter d=0.048 m). The etendue Ω·F of the fiber entrance is calculated from the fiber diameter $d_{fiber} = 400\mu m$ and the solid angle defined by the lens aperture and the distance between lens and fiber (image distance b=0.36 m) to $\Omega \cdot F = 1.75 \cdot 10^{-9}\ m^2 \cdot sr$. Various loss-factors L_i for photons propagating from the fiber entrance to the photocathode of the image intensifier are given in Table 1.

A schematic of the image intensifier tube is shown in Fig. 7. The gain is determined by the quantum efficiency of the (S20-) photocathode ($\eta_{cath} \leq 0.13$), the potential difference over the microchannel plate ($U_{MCP} = 650$ V) and the acceleration voltage to the phosphor screen ($U_{Ph} = 5400\ V$). The image intensifier is operated at low gain because of the high sensitivity of the CCD chip.

The actual intensifier gain is estimated from the value specified by the the manufacturer (luminance gain $G_I = 10^4$ Lambert/Candela at $U_{MCP} = 883V$, $U_{Ph} = 6000\ V$, illumination with white light of 2854 K, cathode response $1.6 \cdot 10^{15}$ electrons/lumen):

Assuming a linear dependence of the phosphor gain G_I on U_{Ph} (P20 phosphor luminance $\simeq$ 12

lumen/Watt(el.), 1 lumen of P20 radiation $\approx 6 \cdot 10^{15}$ photons/s), we obtain the phosphor gain $G_{Ph} = 62$ photons/electron at $U_{ph} = 5400\ V$.

The MCP gain at $U_{MCP} = 883$ V is calculated from the given luminance gain, cathode response and phosphor gain ($G_{Ph}(6000V) = 69$). We obtain $G_{MCP}(883V)$=542 el/el. The actual MCP gain for $U_{MCP} = 650$ V is estimated to G_{MCP} =27 el/el.

The image intensifier exhibits a *spatial nonuniformity* of about ±15%. Fig. 8 shows the relative sensitivity for each channel under standard grouping conditions (gs=20) with respect to the central diode column.

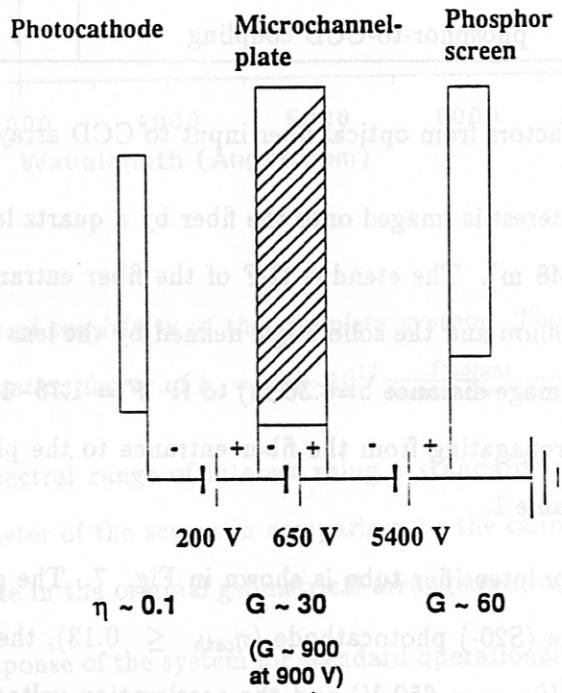

Figure 7: *Schematic of the image intensifier tube. Electrons emitted from the photocathode are multiplied within the microchannels (diameter= 10 μm, center-to-center spacing = 12 μm) and then accelerated against the phosphor screen.*

About 1/7 of the photons emitted from the phosphor screen are imaged onto the CCD-chip surface. Electrons are generated in the storage zone of the CCD pixels with a quantum efficiency

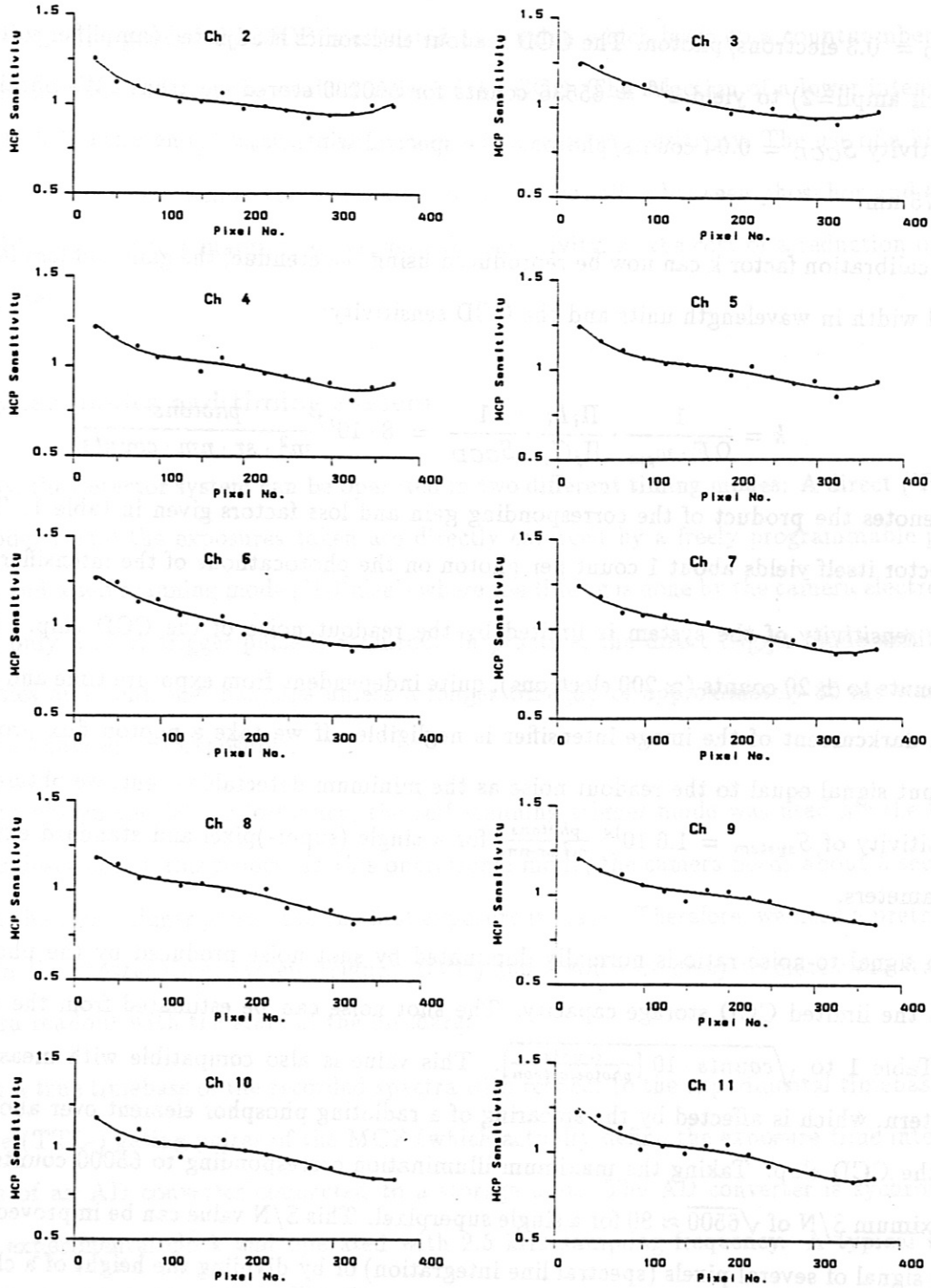

Figure 8: *Relative image intensifier sensitivity for each channel under standard grouping conditions (gs=20) with respect to the central diode column. The solid lines represent polynomial fits used for the software correction.*

$\eta_{CCD} =$ 0.3 electrons/photon. The CCD readout electronics is adjusted (amplifier software gain switch ampli=2) to yield $2^{16} = 65536$ counts for 500000 stored electrons. We obtain a CCD sensitivity $S_{CCD} = 0.04$ counts/photon. The spectral width w_{pix} of one pixel at $\lambda = 450nm$ is 0.0075 nm.

The calibration factor k can now be reproduced using the etendue, the gain and loss factors, the pixel width in wavelength units and the CCD sensitivity:

$$k = \frac{1}{\Omega F \cdot w_{pix}} \cdot \frac{\Pi_i L_i}{\Pi_j G_j} \cdot \frac{1}{S_{CCD}} = 8 \cdot 10^{12} \frac{photons}{m^2 \cdot sr \cdot nm \cdot counts} \tag{2}$$

Π denotes the product of the corresponding gain and loss factors given in table 1. The ICCD detector itself yields about 1 count per photon on the photocathode of the intensifier.

The *sensitivity* of the system is limited by the readout noise of the CCD chip. This noise amounts to $\pm$ 20 counts ($\simeq$ 200 electrons), quite independent from exposure time and groupsize. The darkcurrent of the image intensifier is negligible. If we take a photon flux producing an output signal equal to the readout noise as the minimum detectable event, we obtain a system sensitivity of $S_{system} = 1.6 \cdot 10^{14} \frac{photons}{m^2 \cdot sr \cdot nm}$ for a single (super-)pixel and standard experimental parameters.

The signal-to-noise ratio is normally dominated by shot noise produced by the photocathode and the limited CCD storage capacity. The shot noise can be estimated from the data given in Table 1 to $\sqrt{counts \cdot 10\ [\frac{counts}{photoelectron}]}$. This value is also compatible with measured noise pattern, which is affected by the smearing of a radiating phosphor element over about 3 pixels of the CCD chip. Taking the maximum illumination corresponding to 65000 counts, we get a maximum S/N of $\sqrt{6500} \approx 80$ for a single superpixel. This S/N value can be improved by adding the signal of several pixels (spectral line integration) or by dividing the height of a channel into several sub-superpixels (each of it capable to store the equivalent of 65000 counts) which are individually read out and AD converted at the expense of an increased readout time.

In summary, the photocathode of the image intensifier tube and the readout noise of the CCD have been identified as the most critical elements determining sensitivity and signal-to-noise ratio

of the system. The gain of the MCP is adjusted to a value which leads to a countnumber per photoelectron of the order of the readout noise of the CCD. The selection of a lower intensifier gain would yield a better S/N ratio, at the expense of a reduced sensitivity. The use of a higher image intensifier gain (as well as the installation of a fiber coupling between phosphor and CCD chip) would only lead to a marginal increase of the sensitivity, at the cost of a reduction of the dynamic range.

C. Trigger modes and timing system

Principally, the detector system can be operated in two different timing modes: A direct ('PPG-prog') mode, where the exposures taken are directly enforced by a freely programmable pulse sequence, and a self scanning mode ('1-Pulse') where the timing is done by the camera electronics itself and only a start trigger pulse is required. In practice, the direct trigger mode exhibited irregularities and controller hangups unless a longer timegap of approximately 80 ms was left between two subsequent exposures.

In order to obtain the full performance, the self scanning trigger mode was used for the measurements described in this report. In this operational mode, the camera needs about 3 seconds time from the start trigger pulse until the first exposure is made. Therefore, we need a pretrigger pulse from the central timer system (signal 'DV1') and a software delay to match the start of the camera readout with the start of the discharge.

To obtain a true timebase of the recorded spectra with respect to the experimental timebase, we record the (TTL-) gating pulses of the MCP (which actually define the exposure time interval) by means of an AD converter connected to a storage unit. The AD converter is sychronized with the experimental clock and operated with 2.5 kHz sampling frequency. A typical MCP gating-pulse sequence is shown in Fig. 9

To enhance its lifetime, the MCP is automatically closed by a simple TTL logical circuit as long as no running shot is announced by the central timer system.

A limiting element for the repetition speed of the camera system is given by the persistence of

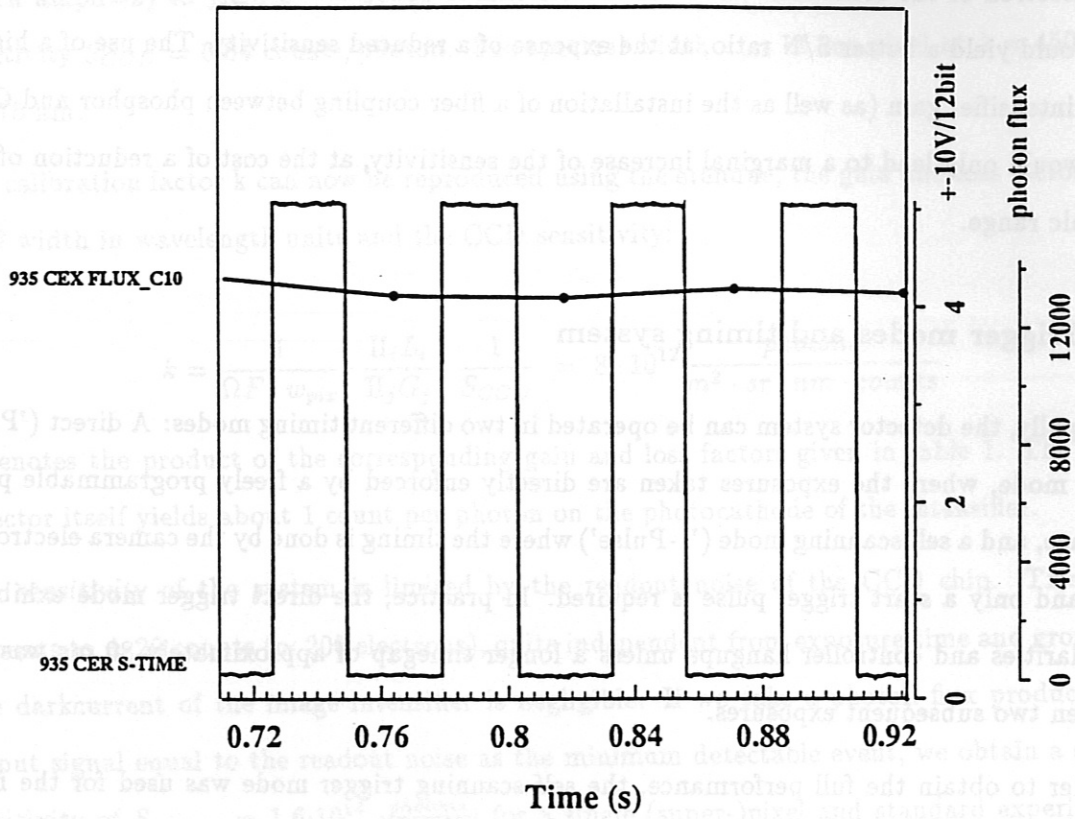

Figure 9: *Time slice of the MCP gating signal and the photon flux integrated over the exposure time. During signal-low, the MCP is gated open. The timevalue of a measured spectrum is taken as the center of the exposure time interval. This signal is automatically used by the evaluation program to calculate the spectroscopic timebase.* $2 \cdot 11$ *windows,* $\tau_{expos} = 30ms$, $\tau_{readout} = 23ms$, $\tau_{cycle} = \tau_{expos} + \tau_{readout}$.

the (P20-) phosphor of the image intensifier. The decay time of the phosphor, which is of the order of a millisecond, can produce ghost spectra at different vertical positions on the chip owing to the CCD readout scheme. The positions of the ghost spectra have a fixed vertical separation from the pixel coordinates of the radiating phosphor. The separation is determined by the number of skipped rows on the chip up to the first readout-row. During the AD-conversion time of this row the decay light of the phosphor is added to those charges which just have reached the corresponding pixel positions in their frame transfer process.
Since the relative contribution of the ghost spectra decreases with increasing exposure time, this effect ist only important for low values of t_{expos}.
When a short exposure time is used, a delay time has to be introduced between the closing of the MCP and the beginning of readout frame transfer. The delay can be easily realized by using the first rows on the chip as dummy-readout rows. The delay-time obtained is about 1 msec per row.

To elucidate the effect of the phosphor persistence, some typical examples for the relative intensity of ghost spectra are given in table 2. In addition to the interfering effect of ghost spectra, the loss of phosphor radiation at the original position leads to reduced signal countrates and a nonlinear detector response.
As a consequence, the sum of exposure- and delay times may not be shorter than about 5 msec to ensure a proper multichordal operation of the detector system.

D. Software

A number of computer programs was written for operation, evaluation and documentation of the diagnostic system. The most important ones are described in the following:

CER
The main operational program written in C and resident on the workstation CER. This program downloads the object code for the camera operation into the camera controller. Parameter values

exposure time (ms)	readout delay (ms)	relative ghost spectrum intensity (%)
1	0	30
1	1	10
1	4	3
10	1	3
100	0	≤ 1

Table 2: Typical relative intensity of a ghost spectrum in comparison to the original signal spectrum for different exposure- and delay times.

for the camera operation like exposure time, channel configuration, groupsizes etc. are read from the file *dsfh* which is edited by the shotfile-editor *sfed*.

cerudc

Interpreter for interactive camera operation. All possible camera commands can be directly sent to the camera controller. The readout of the CCD is visualized on a colour monitor using various graphical tools. Operational instructions, informations about changes in the hardware configuration and calibration are given in the textfile *docfile*.

cerprot

Fortran routine which automatically records the main camera parameters for each shot into the file *cer.prot*.

fluxplot

Fortran routine for plotting the magnetic flux surfaces with respect to the viewing lines of the diagnostic for a given timepoint.

cermain

Fortran program including all routines necessary for the evaluation of recorded spectra. All options like plotting of raw spectra, calibrated spectra, 3-d spectra of the temporal evolution of a single or various chanels, line integration for the calculation of particle fluxes, spatial variation

```
                    CERMAIN  -  Main Input Menue                Vers.  1.03
-------------------------------------------------------------------------------
Use SPC to toggle, Cursor keys, RET and BS to select field, KEYPAD 3 to send
-------------------------------------------------------------------------------
Shot no.     Quit program     Program mode     Timewindow                Level 1
#  935          Continue       Integrate      from  0.000  to  2.200    Yes+store
-------------------------------------------------------------------------------
  No. of 1. scan during or after TS06  -0.360          Atomic mass (amu)
  or, if <0, time difference    begin 1. scan - TS06      12.00
-------------------------------------------------------------------------------
Y-scale (0=auto)  Experiment      Pixel/Data dimen-    Pixelwindow
0.000e+00          AUCD           Phot.+Ang.  sions    from 138    to 172
-------------------------------------------------------------------------------
Line pos. (0=auto)  Gauss Fitwidth  Background        Part. flux   Ions per phot.
  0     (Pixel)        0           710.0(counts)      Yes          6.000e+00
-------------------------------------------------------------------------------
List of Windows:
#1     #2     #3     #4     #5     #7     #8     #9     #10    #11
#0     #0     #0     #0     #0     #0     #0     #0     #0     #0
-------------------------------------------------------------------------------
...............................................................................
Lambda:    4649 Ang.   Exposure time:     30 ms   Tmax:   3.861s

Programmed Windows / Corresponding Channels:    (first 20)
W:    1     2     3     4     5     6     7     8     9    10
C:    2     3     4     5     6    18     7     8     9    10

W:   11     0     0     0     0     0     0     0     0     0
C:   11     0     0     0     0     0     0     0     0     0
```

Figure 10: *Main input menu for the evaluation program cermain. All possible program features can be selected easily by toggling. In the lower part of the menu, informations about the main camera parameters are displayed.*

of fluxes and polynomial-, single- and multigaussian fits can be selected by an input mask menu, as shown in Fig. 10.

The generation of level-1 shotfile data is also possible. Two pages of the shotfile header used for the storage of particle fluxes under the diagnostic name CEX are shown in Fig. 11.

For multigaussian fits, the application of reasonable starting parameters is desired. This can easily be done interactively with the mouse using the reply menu of the pplot graphics package. The example in Fig. 12 shows a Zeeman triplet, whose splitting can be used to determine the strength of the magnetic field at the location of the spectral line emission.

The evaluation program *cermain* is resident on the workstations CER and SLCAXK (SUN Spar-

```
Press <PF1> for help
                Object    CEX                    Type    DIAGNOSTIC

    text   particle flux from inner wall from CER diagnostic

    level   1          status   0          error code      0

    <------------------------- relations ---------------------------------->

    ?       ?       ?       ?       ?       ?       ?       ?

    address of data block        820    length of data block      2bc0

    Experiment                 PRIV

    Diagnostic Code            CEX                  Upper limit          256 * 4K

    Diagnostic Type            Autonom              Number of Objects     16

    Shot Type                  NormalShot           DSFH Version           4
```

```
Press <PF1> for help

                    Press <HELP> to get Keys
Name      Obj-Type                  Remarks
-----------------------------------------------------------------------------
CEX       DIAGNOSTIC particle flux from inner wall from CER diagnostic
SIGNALS   LIST       List of all Signals, Signal Groups and Time Bases
T-CEX     TIME_BASE
FLUX_C01  SIGNAL     particle flux  CER channel 1  lowest position
FLUX_C02  SIGNAL     particle flux  CER channel 2
FLUX_C03  SIGNAL     particle flux  CER channel 3
FLUX_C04  SIGNAL     particle flux  CER channel 4
FLUX_C05  SIGNAL     particle flux  CER channel 5
FLUX_C06  SIGNAL     particle flux  CER channel 6
FLUX_C07  SIGNAL     particle flux  CER channel 7
FLUX_C08  SIGNAL     particle flux  CER channel 8
FLUX_C09  SIGNAL     particle flux  CER channel 9
FLUX_C10  SIGNAL     particle flux  CER channel 10
FLUX_C11  SIGNAL     particle flux  CER channel 11
FLUX_C12  SIGNAL     particle flux  CER channel 12  midplane
FLUX_C99  SIGNAL     particle flux  CER special channel
```

Figure 11: *Example for a shotfile header used to generate and store level-1 data of particle fluxes.*

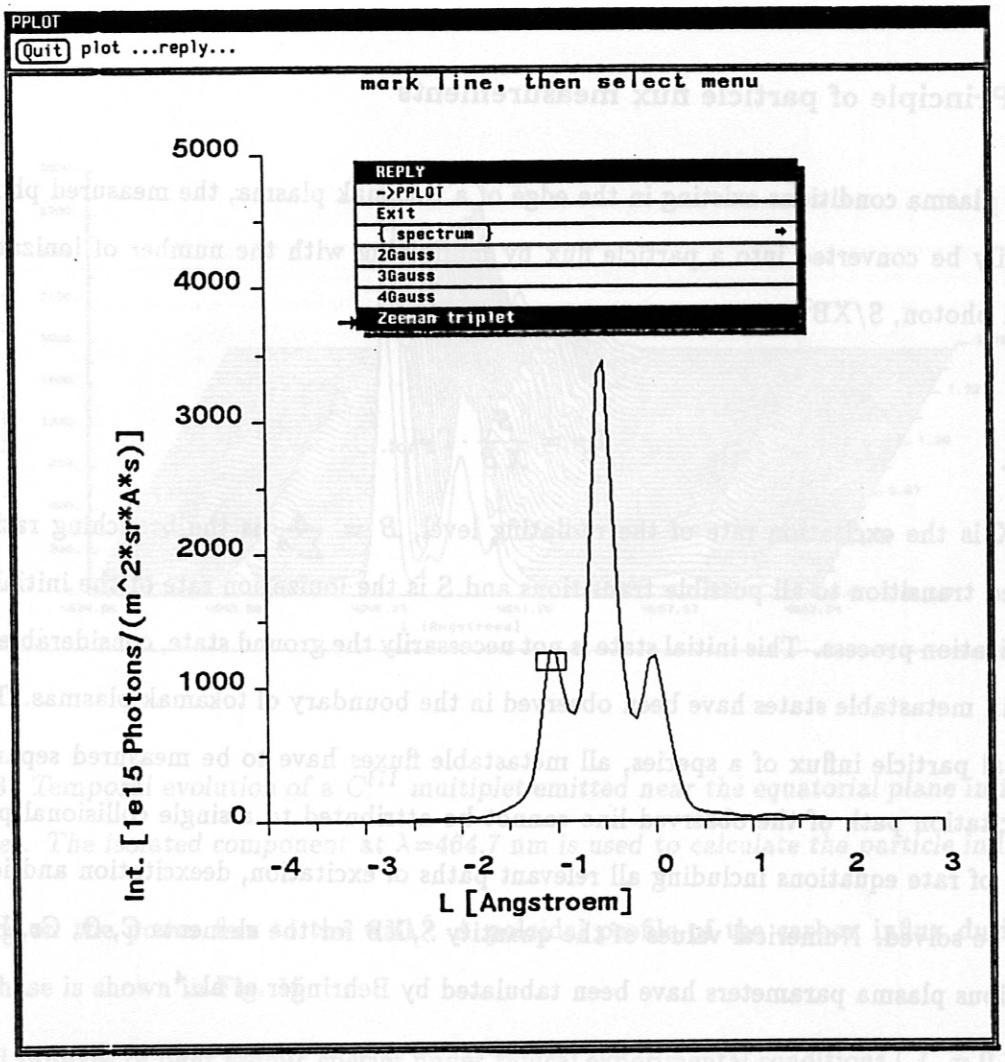

Figure 12: *Menu for multigaussian fits to be selected by the mouse. The position, height and width of the individual line components is marked by rectangles.*

c). System parameters concerning hardware configuration of channels and calibration parameters are stored in the files *arrange.dat* and *calibration.dat* in the *parameter* directory. Copies of the parameter files valid for the 1991 period are printed in the appendix.

III. Principle of particle flux measurements

For the plasma conditions existing in the edge of a tokamak plasma, the measured photon flux can easily be converted into a particle flux by muliplying with the number of ionizations per emitted photon, S/XB[3]:

$$\Gamma_P = \frac{S}{XB} \cdot \Gamma_{Phot.} \tag{3}$$

Here, X is the excitation rate of the radiating level, $B = \frac{A}{\sum A}$ is the branching ratio of the observed transition to all possible transitions and S is the ionization rate of the initial state of the excitation process. This initial state is not necessarily the ground state, considerable fluxes of atoms in metastable states have been observed in the boundary of tokamak plasmas. To obtain the total particle influx of a species, all metastable fluxes have to be measured separately. If the excitation path of the observed line cannot be attributed to a single collisional process, a system of rate equations including all relevant paths of excitation, deexcitation and ionization has to be solved. Numerical values of the quantity S/XB for the elements C, O, Cr, Fe and Ni for various plasma parameters have been tabulated by Behringer et al..[4]

IV. Experimental results

As an experimental example, the temporal evolution of the C^{III}-multiplet al λ=465 nm emitted near the equatorial plane in front of the limiter for a circular limiter discharge is shown in Fig. 13. The temporal variation of the metastable C^{2+} (2s2p $^3P^o$) influx calculated from the spectra of Fig. 13 is compared to the evolution of plasma current and density in Fig. 14. The influx of sputtered carbon is nearly proportional to the plasma current, owing to the dependence of

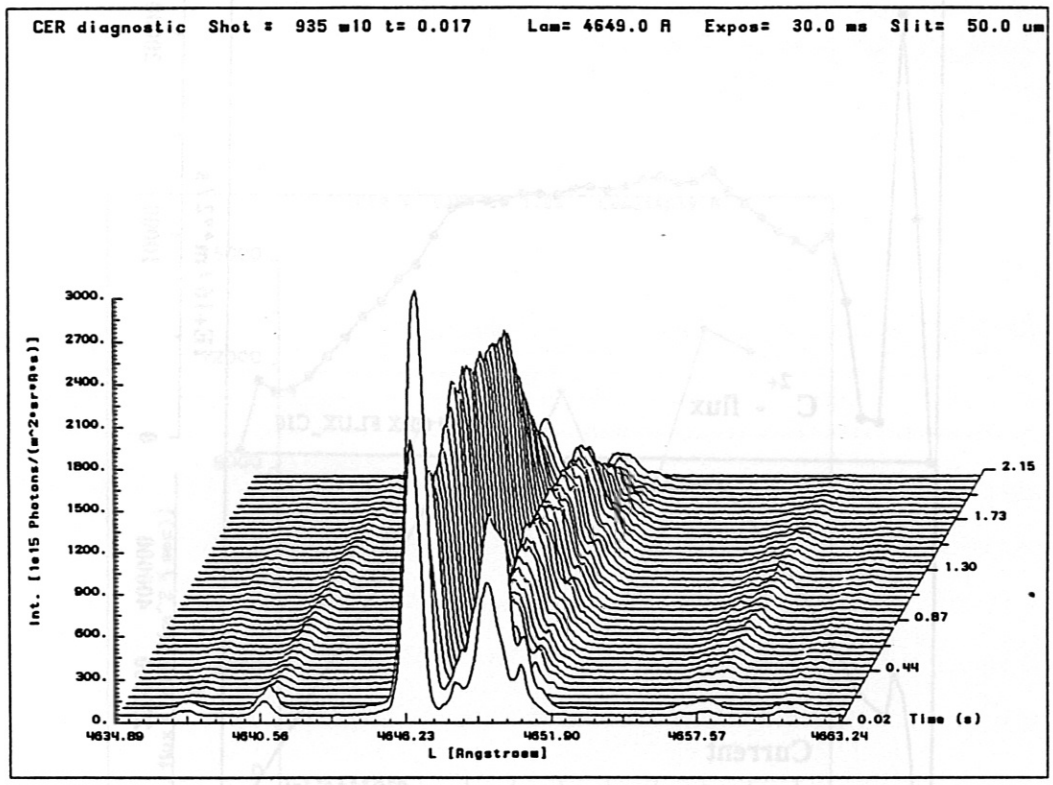

Figure 13: *Temporal evolution of a C^{III} multiplet emitted near the equatorial plane in front of the limiter. The isolated component at λ=464.7 nm is used to calculate the particle influx.*

sputtering on the power flux to the wall.[5] A poloidal profile of the carbon influx during the flattop phase is shown in Fig. 15.

Measured influxes of light atomic species under typical experimental conditions ($I_p = 0.35MA$, $\overline{n}_e = 2 \cdot 10^{19}\ m^{-3}$, helium limiter plasma) are given in table 3. The values of S/XB, which depend moderately on the temperature and slightly on the density, were taken for typical, estimated experimental edge conditions ($T_e \approx 80\ eV$, $n_e \approx\ 5 \cdot 10^{18}\ m^{-3}$). The hydrogen released from the wall originates from conditioning glow discharges or an original deposition in the graphite tiles. The tokamak had never experienced a hydogen-filled plasma discharge before.

A strong reduction of the impurity influx from the inner wall occurs during divertor operation. This is demonstrated in Fig. 16, where the influx of O^+ ($2s^2sp^3\ ^2D$) is plotted in comparison

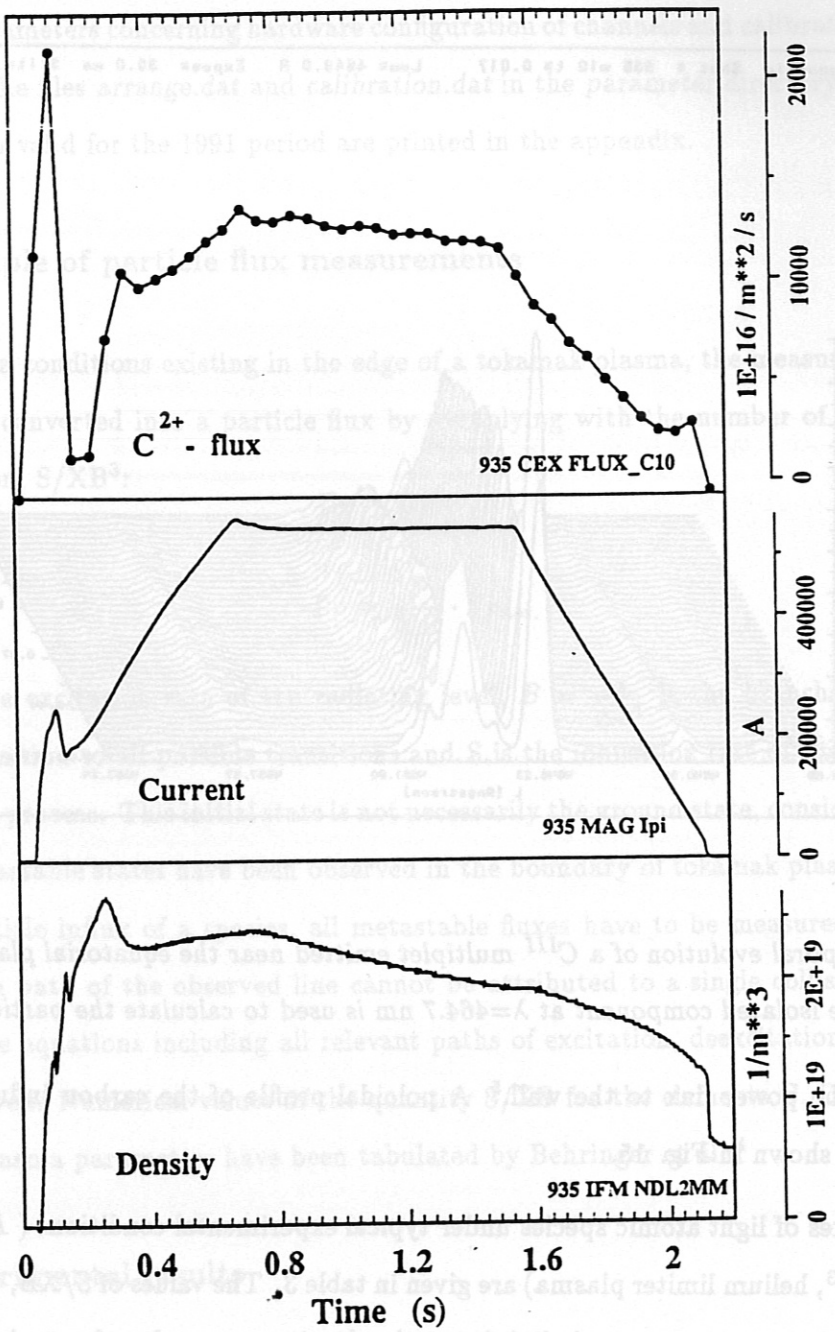

Figure 14: *Temporal evolution of the metastable C^{2+} $(2s2p\,^3P^o)$ influx, in units of $10^{16}\ m^{-2}\cdot s^{-1}$ in comparison to plasma current and density. Except a turbulent phase at the beginning of the discharge, the sputtered carbon flux is approximately proportional to the plasma current.*

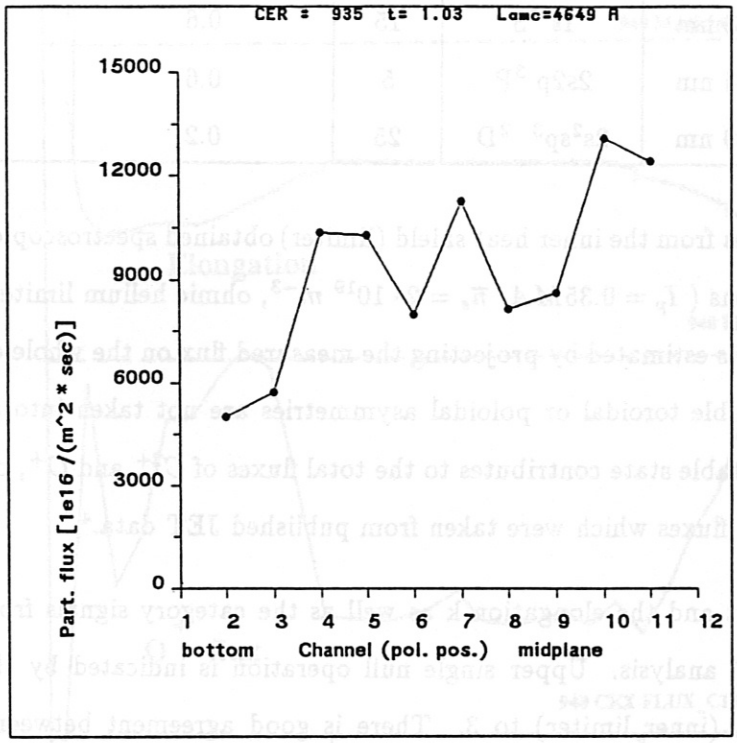

Figure 15: *Poloidal profile of the C^{2+} influx during the flattop phase of the discharge shown in Fig. 14. Channel 2 views to the bottom of the heat shield, channel 10 views approximately to its center. The exact path of the viewing lines with respect to the last closed flux surface is shown in Fig. 3. $I_p = 0.55MA$, $\overline{n}_e = 2.3 \cdot 10^{19}\ m^{-3}$,*

species	transition	metastable state	$\frac{S}{XB}$	flux $[10^{20}\ m^{-2} \cdot s^{-1}]$	est. total flux $[10^{20}\ s^{-1}]$
He^+	468.57 nm	1s ^{2}S	50	5	40
H^0	656.28 nm	1s ^{2}S	15	0.6	4.8
C^{2+}	464.74 nm	2s2p ^{3}P	5	0.6	8
O^+	441.49 nm	2s^{2}sp^3 ^{2}D	25	0.2	4

Table 3: Particle fluxes from the inner heat shield (limiter) obtained spectroscopically for typical experimental conditions ($I_p = 0.35MA$, $\overline{n}_e = 2 \cdot 10^{19}\ m^{-3}$, ohmic helium limiter plasma). The total flux of a species is estimated by projecting the measured flux on the whole effective limiter surface (8 m^2). Possible toroidal or poloidal asymmetries are not taken into account. Since more than one metastable state contributes to the total fluxes of C^{2+} and O^+, multipliers were applied to the partial fluxes which were taken from published JET data.[4]

to the plasma current and the elongation k as well as the category signals from the function parametrization (FP) analysis. Upper single null operation is indicated by the jump of the signal ikCAT from 1 (inner limiter) to 3. There is good agreement between the indicated divertor transition and the lifting of the plasma off the limiter detected by the reduction of oxygen released. The two different signals ikCAT (diagnostics FPG and FPH) were obtained with slightly different plasma currents. The comparison with the measured impurity influx recommends the use of the FPH diagnostic (there are other other considerations to rely on the plasma current IpiFP used in FPH).

During the current ramp-up of a discharge, frequently a temporary reduction of the impurity influx is observed (see, e.g. Fig. 14 at t=0.2 sec.). To investigate, wether this behaviour can be attributed to a detachment[6] of the plasma from the limiter, we determined the position of the spectral line emission of the He^0 (3d^{3}D- 2p^{3}P) transition by means of the Zeeman splitting and the known magnetic field. This particular transition exhibits a well resolved Zeeman pattern which is evaluated in the Paschen-Back regime[7] neglecting the small fine structure splitting.

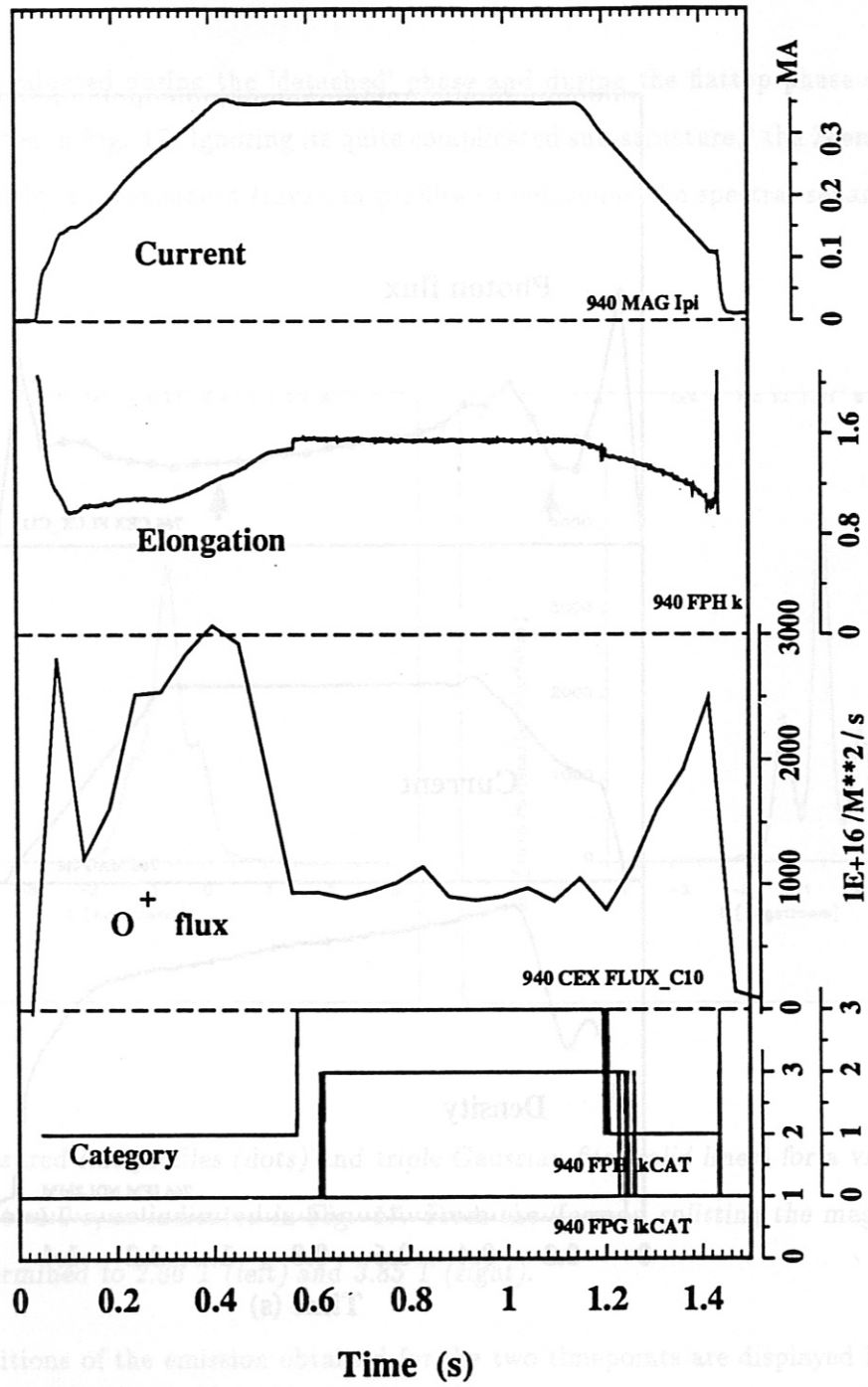

Figure 16: *Temporal development of plasma current, elongation, O^+ ($2s^2sp^3\ ^2D$) influx and discharge category from the FP analysis using two slightly different parameter sets. A pronounced reduction of the impurity influx from the inner wall occurs during divertor operation. Flattop current is 0.35 MA, oxygen influx in units of $10^{16}\ m^{-2} \cdot s^{-1}$.*

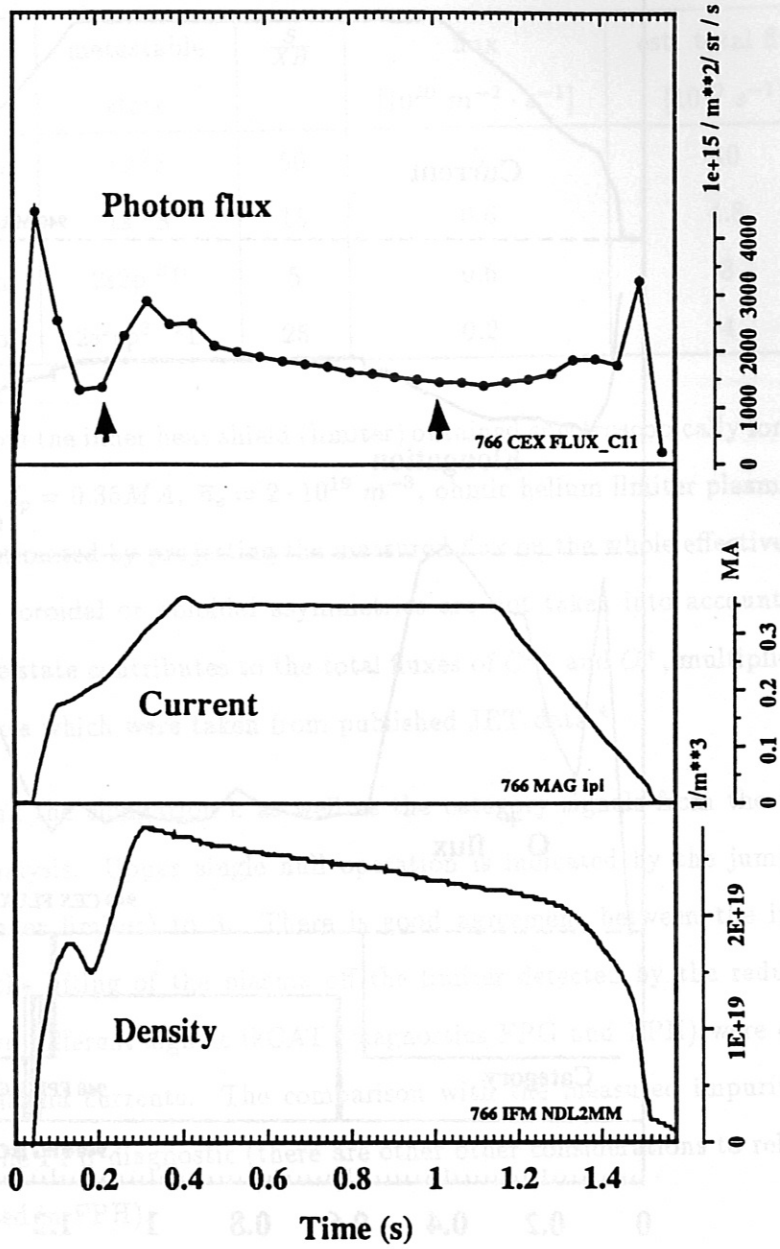

Figure 17: *Temporal development of the photon flux in the transition* He^0 *(*$3d^3D$*-* $2p^3P$*) at* λ *= 587.6 nm. Circular limiter plasma, flattop values are* $I_p = 0.35MA$, $\overline{n}_e \approx 2 \cdot 10^{19}\ m^{-3}$. $B_t(R_0$*=1.65 m) = 2.5 Tesla. Zeeman splittings are evaluated for the two marked timepoints.*

Splittings were evaluated during the 'detached' phase and during the flattop phase of the discharge, as indicated in Fig. 17. Ignoring its quite complicated sub-structure,[8] the Zeeman triplet was simply fitted by 3 independent Gaussian profiles to determine the spectral separation (see Fig. 18).

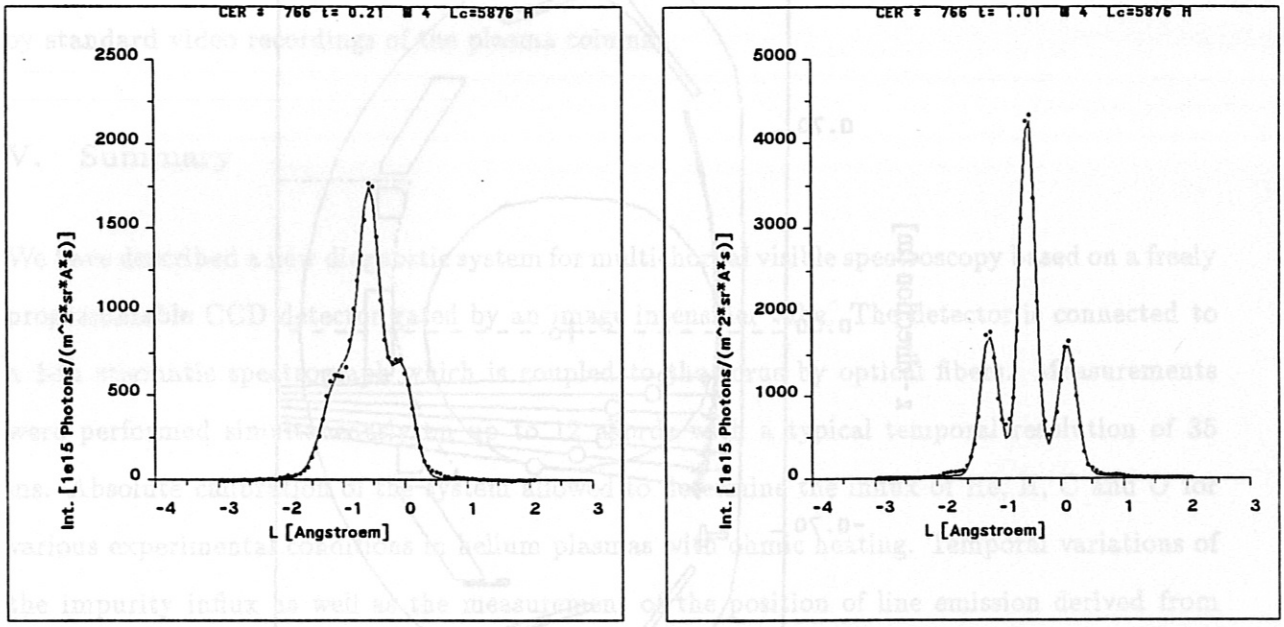

Figure 18: *Measured line profiles (dots) and triple Gaussian fits (solid lines) for a viewing line at t=0.2 s and t=1.0 s, as indicated in Fig. 17. From the Zeeman splitting the magnetic field strength is determined to 2.86 T (left) and 3.85 T (right).*

The spatial positions of the emission obtained for the two timepoints are displayed in Fig. 19, where also the last closed flux surface for the flattop phase is shown. The group of observed positions during the early discharge phase indicates a shrunk minor plasma radius ('detached plasma'). The shrinking may be due to high impurity content and edge cooling in combination with high values of q_Ψ. During the flattop phase, the emission occurs just on the limiter surface (It should be noted, that the emission before the event, at t=0.1 s, is located about 12 cm in front of the limiter). The positions are formally calculated from the Zeeman splittings, no attempt

was made to determine their spatial extent from the data. However, the marked separation of the Zeeman pattern emitted during the flattop phase indicates a quite localized emission spot, while the early profile exhibits some smearing.

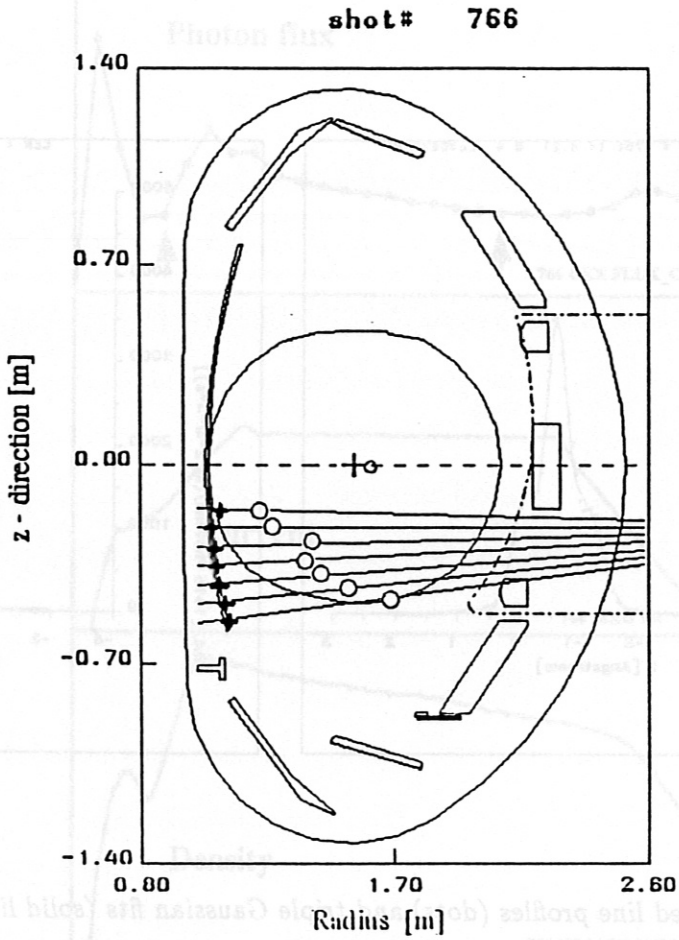

Figure 19: *Positions of spectral line emission for the two timepoints of the discharge indicated in Fig. 17. During the flattop phase, the emission is located at the limiter (crosses), while a shrinked minor radius is observed during the phase of reduced line radiation at t=0.2 s (circles). The last closed flux surface is shown for the flattop phase.*

Despite the straightly enforced interpretation of the Zeeman pattern, a problem arises when we ask for the physical origin of the line excitation. During the 'detached' phase, the mechanism of excitation seems to be the standard impact by thermal electrons. For the flattop phase,

however, especially the lower part of the limiter is too far away from the plasma boundary to see an electron temperature high enough for the impact excitation from the ground state. A possible explanation allowing excitation energies highly above the thermal energy of the electrons at the limiter may be the recombination of He^+ into excited states or the excitation from the metastable Helium triplet state, where electron energies of a few eV are sufficient.
The positions of the emitting plasma layer determined from the Zeeman splitting are confirmed by standard video recordings of the plasma column.

V. Summary

We have described a new diagnostic system for multichordal visible spectroscopy based on a freely programmable CCD detector gated by an image intensifier tube. The detector is connected to a 1-m stigmatic spectrograph which is coupled to the torus by optical fibers. Measurements were performed simultaneously on up to 12 chords with a typical temporal resolution of 35 ms. Absolute calibration of the system allowed to determine the influx of He, H, C and O for various experimental conditions in helium plasmas with ohmic heating. Temporal variations of the impurity influx as well as the measurement of the position of line emission derived from Zeeman splitting are used to detect changes of the plasma configuration.

VI. Acknowledgement

We are grateful to Dr. G. Fussmann and Dr. U. Schumacher for helpful discussions as well as to A. Troendle for technical support.

VII. Appendix

Parameter file describing hardware configuration for the 1991 shot period.

```
Jul 31 12:26 1991  arrange.dat Page 1


CER - System fiber arrangement file                    last update  16.07.91
---------    put the newest arrangement on top position -----------------

             first row of data block  valid since 11.06.91
557 55     AVGD shotno  and AXK shotno data are valid from
24         number of items
channel no      lower pos    upper pos     fiber name
  1               1            29            F1
 13               31           33            E1
  2               35           75            F2
 14               77           79            E2
  3               81           121           F3
 15               124          126           E3
  4               129          169           F4
 16               171          173           E4
  5               175          215           F5
 17               217          219           E5
  6               222          262           F6
 18               264          266           E6
  7               269          309           F7
 19               311          313           E7
  8               315          355           F8
 20               357          359           E8
  9               362          402           F9
 21               404          406           E9
 10               408          448           F10
 22               450          452           E10
 11               454          494           F11
 23               497          499           E11
 12               501          541           F12
 24               544          546           E12
                     first row of data block  created 16.07.91
1   1      AVGD shotno  and AXK shotno data are valid from
1          number of items
channel no      lower pos    upper pos     fiber name
  1               1            576           all
```

Parameter file describing the absolute calibration for the 1991 shot period.

```
*Dec  2 19:30 1991  calibration.dat Page 1

CER - System calibration parameter file                last update  02.12.91
---------    put the newest arrangement on top position ----------------

             first row of data block  valid since 11.06.91
557 55     AUGD shotno  and AXK shotno data are valid from
9.95e14     (phot/(m^2*sr*A*s * counts/ms))  norm calibration factor
24          number of channels
channel no      weighting factor  polynom coeffs. for MCP sensitivity
1                 1.              0.       0.       0.     0.
2                 1.180          -5.462e-4  -1.863e-6  -6.58e-9   2.064e-10
3                 1.056          -8.305e-4   2.753e-6  -3.62e-10  5.211e-11
4                 0.575          -7.664e-4  -4.352e-6  -8.51e-9   2.259e-10
5                 0.966          -6.829e-4  -3.318e-6  -1.078e-8  2.135e-10
6                 0.894          -1.052e-3   6.125e-7  -3.424e-9  8.673e-11
7                 1.274          -9.560e-4  -2.675e-6  -3.986e-9  1.650e-10
8                 1.274          -8.864e-4  -5.102e-6  -4.514e-9  2.023e-10
9                 1.258          -5.832e-4  -2.729e-6  -1.776e-8  1.316e-10
10                1.246          -5.850e-4  -5.408e-6  -1.410e-8  1.932e-10
11                0.70           -7.687e-4  -4.721e-6  -1.562e-8  2.239e-10
12                1.0            -7.154e-4  -5.241e-7  -1.403e-8  1.296e-10
13                1.              0.       0.       0.     0.
14                1.              0.       0.       0.     0.
15                1.              0.       0.       0.     0.
16                1.              0.       0.       0.     0.
17                1.              0.       0.       0.     0.
18                1.              0.       0.       0.     0.
19                1.              0.       0.       0.     0.
20                1.              0.       0.       0.     0.
21                1.              0.       0.       0.     0.
22                1.              0.       0.       0.     0.
23                1.              0.       0.       0.     0.
24                1.              0.       0.       0.     0.

 -35.06  22.324  -5.079  0.4893  -0.0174   pol. coef. for wavelength dependence
 0.  0. 0.        polynom coefficients detector nonlinearity

             first row of data block  valid since 01.01.91
1  1        AUGD shotno  and AXK shotno data are valid from
8.5e14      (phot/(m^2*sr*A*s * counts/ms))  norm calibration factor
1           number of channels
channel no      weighting factor  polynom coeffs. for MCP sensitivity
1                 1.              0.       0.       0.     0.

 0.  0. 0. 0. 0.    polynom coefficients for wavelength dependence
 0.  0. 0.        polynom coefficients detector nonlinearity

end of file
```

References

[1]GRUBER, O., KAUFMANN, M., KÖPPENDÖRFER, W., LACKNER, K., and NEUHAUSER, J., Journal of Nuclear Materials **121** (1984) 407.

[2]IDA, K., private communication, 1991.

[3]FUSSMANN, G., HOFMANN, J. V., JANESCHITZ, G., and YANG, H. R., Nucl. Fusion **30** (1990) 2319.

[4]BEHRINGER, K., SUMMERS, H. P., DENNE, B., FORREST, M., and STAMP, M., Plasma Phys. Controlled Fusion **31** (1989) 2059.

[5]PITCHER, C. S., BUDNY, R. V., HILL, K. W., et al., Journal of Nuclear Materials **176** (1990) 285.

[6]STRACHAN, J. D., BOODY, F. P., BUSH, C. E., et al., Journal of Nuclear Materials **145-147** (1987) 186.

[7]SHORE, B. W. and MENZEL, D. H., *Principles of ATOMIC SPECTRA*, John Wiley and Sons, Inc., New York, 1968.

[8]CAROLAN, P. G., FORREST, M. J., PEACOCK, N. J., and TROTMAN, D. L., JET-P(85)05 (1985).